Exploring Integrability-Chaos Transition with a Sequence of Independent Perturbations

Vladimir A. Yurovsky◉
School of Chemistry, Tel Aviv University, 6997801 Tel Aviv, Israel

A gas of interacting particles is a paradigmatic example of chaotic systems. It is shown here that, even if all but one particle are fixed in generic positions, the excited states of the moving particle are chaotic. They are characterized by the number of principal components (NPC)—the number of integrable system eigenstates involved into the nonintegrable one, which increases linearly with the number of strong scatterers. This rule is a particular case of the general effect of an additional perturbation on the system chaotic properties. The perturbation independence criteria supposing the system chaoticity increase are derived here as well. The effect can be observed in experiments with photons or cold atoms as the decay of observable fluctuation variance, which is inversely proportional to NPC and, therefore, to the number of scatterers. This decay indicates that the eigenstate thermalization is approached. The results are confirmed by numerical calculations for a harmonic waveguide with zero-range scatterers along its axis.

Evolution of integrable systems is completely predictable, and, according to the Kolmogorov-Arnold-Moser theorem (see [1]), weak perturbations do not affect this property. There are numerous examples of such classical and quantum systems, including stellar mechanics, hydrogen atoms, and many-body systems, both realized in experiments, such as the quantum Newton cradle [2,3] and cold-atom breathers [4,5] (see [6–9] for the theoretical description) and those waiting for realization [10].

When the integrability-lifting perturbation is sufficiently strong, the system evolution becomes unpredictable. Nevertheless, a completely chaotic system relaxes to a state described by the Gibbs ensemble, thanks to the eigenstate thermalization mechanism—eigenstate expectation values are equal to microcanonical averages at the eigenstate energy—introduced in Refs. [11,12] (see also [13,14], the experimental work [15], the review [16], and the references therein). In contrast, integrable systems relax to states described by the generalized Gibbs ensemble [17–21].

However, a generic system lies between integrable and completely chaotic systems [22–49]. The incomplete chaos can be related to weak integrability-lifting perturbations [29,31,32,34,47,48] or phase-space separation in both classical and quantum systems. It can have also a specific quantum nature, such as many-body localization [33,37,49] or zero-range interactions [22–24,26–28,30]. Chaoticity of such incompletely chaotic systems can be characterized by the inverse participation ratio (IPR) [28,31,33,50]. Its inverse—the number of principal components (NPC)—estimates the number of integrable system eigenstates comprising the nonintegrable one. IPR ranges from 1 for integrable systems to 0 for completely chaotic ones. It governs the expectation values after relaxation in incompletely chaotic systems with no selection rules [28,31].

This regularity has been confirmed in different systems [41]. The fluctuations of expectation values over eigenstates are strong for integrable systems and vanish in completely chaotic ones, according to the eigenstate thermalization hypothesis. These fluctuations, too, are governed by IPR [32].

Exploration of the integrability-eigenstate thermalization crossover is of special interest, and the means of the system chaoticity prediction based on its Hamiltonian, with no numerical calculations, would be very useful. The exponential decay of fluctuations in many-body systems with the number of particles was predicted in Ref. [12]. However, this sharp decay complicates the exploration due to the high sensitivity of the system chaoticity to the number of particles. Analytical predictions for single particles with random-matrix perturbations (see [31] and the references therein) are applicable to strong perturbations (and chaos) only. The system chaoticity can be modified by an additional perturbation; e.g., it can transform an integrable system into a chaotic one. However, the effect of an additional perturbation on a chaotic system is ambiguous; e.g., the system integrability can be restored if the additional perturbation is equal to the integrability-lifting one with opposite sign. The system chaoticity increases when the additional perturbation obeys the independence criteria determined here. Then, a linear increase of NPC with the number of independent perturbations of the same shape is predicted. Simultaneous decay of expectation value fluctuations indicates that the eigenstate thermalization is approached. These predictions are confirmed by numerical calculations for a harmonic waveguide with zero-range scatterers along its axis. Both NPC and expectation value fluctuations are specific characteristics of quantum chaos, and it is unclear if they have classical counterparts.
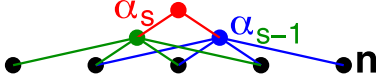
FIG. 1. A chart of connection between eigenstates. The number of the integrable system eigenstates **n** connected to the non-integrable ones increases from 4 to 5 due to an additional perturbation.

Consider a sequence of Hamiltonians $\hat{H}_s = \hat{H}_0 + \sum_{s'=1}^{s} \hat{V}_{s'}$. Here, the integrable one $\hat{H}_0$ has the eigenstates $|\mathbf{n}\rangle$ and eigenenergies $E_{\mathbf{n}}$ labeled by a proper set of integrals of motion **n**. The integrability is lifted by the perturbations $\hat{V}_{s'}$. The eigenstates $|\alpha_s\rangle$ of the nonintegrable Hamiltonians $\hat{H}_s$ are labeled in the increasing order of their eigenenergies E_{α_s}. If $\hat{H}_s$ is invariant under some transformations, sets of $|\alpha_s\rangle$ with certain symmetry have to be considered separately. For example, there may be eigenstates with certain angular momentum for rotational symmetry of $\hat{H}_s$, or certain parity for inversion invariance, or certain quasimomentum for spatial periodicity. Such sets of eigenstates can be described by different Hamiltonians, e.g., with separated angular momentum for rotational symmetry, or restricted to the unit cell for spatial periodicity. Such Hamiltonians can contain fewer perturbations than the original one $\hat{H}_s$. Only the case when all $\hat{H}_s$ have the same invariance group is considered.

Each eigenstate $|\alpha_s\rangle$ can be expanded in terms of $|\mathbf{n}\rangle$, and the strength function

$$W_s(E_{\mathbf{n}}, E_{\alpha_s}) = \langle |\langle \mathbf{n}|\alpha_s\rangle|^2\rangle \tag{1}$$

is the probability averaged over states with a fixed energy difference (see [51]). The relation between the strength functions for $|\alpha_s\rangle$ and $|\alpha_{s-1}\rangle$,

$$W_s(E_{\mathbf{n}}, E_{\alpha_s}) \approx \sum_{E_{\alpha_{s-1}}} W_{s-1}(E_{\mathbf{n}}, E_{\alpha_{s-1}})\langle |\langle \alpha_{s-1}|\alpha_s\rangle|^2\rangle, \tag{2}$$

is obtained (see [51]) neglecting the interference terms. This approximation is applicable whenever the perturbation $\hat{V}_s$ is independent of $\hat{V}_{s'}$ with $s' < s$, i.e.,

$$\sum_{\mathbf{n},\mathbf{n}'} \langle \mathbf{n}|\hat{V}_s|\mathbf{n}'\rangle\langle \mathbf{n}'|\hat{V}_{s'}|\mathbf{n}\rangle \ll \sum_{s''}\sum_{\mathbf{n},\mathbf{n}'} |\langle \mathbf{n}|\hat{V}_{s''}|\mathbf{n}'\rangle|^2. \tag{3}$$

The summations over **n** and **n**′ in the microcanonical interval (see [51]) lead to the Berry autocorrelation function [56]. It is localized within the characteristic de Broglie wavelength determined by the characteristic eigenstate energy. Condition (3) is satisfied, for example, if the spatial separation between local potentials exceeds the characteristic de Broglie wavelength (see [51]). (The effect of spatially separated perturbations on certain characteristics

of energy spectra was analyzed in Ref. [57].) Other examples are the angular-dependent potentials with no common spherical harmonics in their expansions, such as different terms in multipole expansion, and the potentials of different parity (see [51]).

The relation (2) means that an addition of an independent perturbation increases the number of the integrable system eigenstates involved to the nonintegrable one (see Fig. 1). This intuitive picture illustrates the quantitative relation presented below.

Since $W_s(E_{\mathbf{n}}, E_{\alpha_s})$ should decay as $(E_{\mathbf{n}} - E_{\alpha_s})^{-2}$ in the limit $|E_{\mathbf{n}} - E_{\alpha_s}| \to \infty$ (see [51]) but has no singularities as $E_{\mathbf{n}}$ and E_{α_s} never coincide, the Lorentzian profile

$$W_L(E, \Gamma) = \frac{1}{\pi}\frac{\Gamma}{E^2 + \Gamma^2} \tag{4}$$

is a natural choice for the continuous strength function $W_s(E_{\mathbf{n}}, E_{\alpha_s}) \approx W_L(E_{\alpha_s} - E_{\mathbf{n}}, \Gamma_s)\Delta E$. Here, ΔE is the average difference between eigenenergies in the vicinity of E_{α_s}. Such a strength function has been applied to systems with strong random-matrix perturbations [31,58–61], when the profile contains many energy levels and Γ can be evaluated using the Fermi golden rule. On the integrability-chaos crossover, explored here, the profile may contain only a few levels and the Fermi golden rule can be inapplicable, but the strength function with some Γ retains the necessary properties. The averaged IPR $\eta_s \equiv \sum_{\mathbf{n}} \overline{|\langle \alpha_s|\mathbf{n}\rangle|^4}^{\alpha_s}$ (where the overbar means the microcanonical average over the states α_s) is related to the Lorentzian width Γ_s as (see [51])

$$\eta_s = \begin{Bmatrix} 2 \\ 3 \end{Bmatrix} \frac{\Delta E}{2\pi\Gamma_s}, \tag{5}$$

where the factor 3 is chosen for the time-reversal (T) invariant and PT-invariant systems (where P is the inversion) and 2 is chosen otherwise. For the fixed integrable Hamiltonian $\hat{H}_0$ determining the energy difference ΔE, Eq. (5), together with the relation $\Gamma_s = \Gamma_{s-1} + \Gamma'$ (see [51]), leads to the recurrence relation for NPC η_s^{-1}:

$$\eta_s^{-1} = \eta_{s-1}^{-1} + \nu. \tag{6}$$

The parameter ν is approximately independent of s if the chaotic properties of $|\alpha_s\rangle$ weakly depend on s and the shape of $\hat{V}_s$ is independent of s (as for strong scatterers with the same strength). Then, Eq. (6) provides a linear dependence $\eta_s^{-1} = \eta_2^{-1} + (s - 2)\nu$ of NPC on the number of scatterers. An additional independent perturbation increases NPC even if its value is so high that the system can be considered as a completely chaotic one.

The prediction (6) is tested for models where the integrability of a particle in a potential with separable
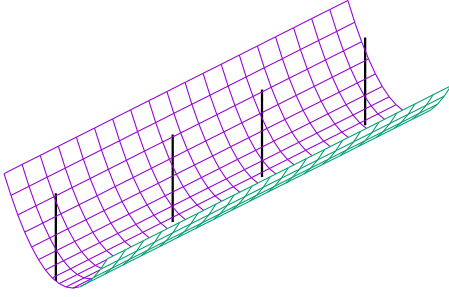
FIG. 2. Harmonic waveguide with four zero-range scatterers along its axis.

coordinates is lifted by s fixed zero-range scatterers. Other examples of such models are flat orthogonal billiards—multiscatterer generalizations of the Seba billiard [22]. Their energy spectrum properties were analyzed for up to six scatterers [23,24,43]. Scattering in a harmonic potential was analyzed in Ref. [62]. The set of scatterers is a particular case of the rank-s separable potential $\hat{V}_{s'} = V_{s'}|\mathcal{F}_{s'}\rangle\langle\mathcal{F}_{s'}|$ with the form factors $|\mathcal{F}_{s'}\rangle$. For such potentials, the eigenstate expansion coefficients can be expressed as (see [51])

$$\langle\mathbf{n}|\alpha_s\rangle = \sum_{s'=1}^{s} V_{s'} \frac{\langle\mathbf{n}|\mathcal{F}_{s'}\rangle\langle\mathcal{F}_{s'}|\alpha_s\rangle}{E_{\alpha_s} - E_{\mathbf{n}}} \qquad (7)$$

in terms of s overlaps $\langle\mathcal{F}_{s'}|\alpha_s\rangle$ which obey the set of linear equations

$$\sum_{s''=1}^{s} \left(V_{s''} \sum_{\mathbf{n}} \frac{\langle\mathcal{F}_{s'}|\mathbf{n}\rangle\langle\mathbf{n}|\mathcal{F}_{s''}\rangle}{E_{\alpha_s} - E_{\mathbf{n}}} - \delta_{s''s'} \right) \langle\mathcal{F}_{s''}|\alpha_s\rangle = 0. \qquad (8)$$

This system has nontrivial solutions if the determinant of its matrix is equal to zero. Then the eigenenergies E_{α_s} are roots of the determinant. High-rank separable potentials can also approximate long-range, e.g., dipole-dipole, ones [63]. This approximation was used for energy spectra calculation [64].

The present models are generalizations of the single-scatterer model [26–28,30]. The integrable Hamiltonian contains the kinetic energy and the radial harmonic potential with the frequency $\omega_\perp$:

$$\hat{H}_0 = \frac{\hbar^2}{2m}\left[\left(\frac{1}{i}\frac{\partial}{\partial z} - A\right)^2 - \triangle_\rho \right] + \frac{m\omega_\perp^2\rho^2}{2}, \qquad (9)$$

where z and ρ are the axial and radial coordinates, respectively, m is the particle mass, and A is a vector potential. The discrete energy spectrum is provided either by the periodic boundary conditions (PBCs), $\langle z + L|\alpha_s\rangle = \langle z|\alpha_s\rangle$, or by a hard-wall box, $\langle z=0|\alpha_s\rangle = \langle z=L|\alpha_s\rangle = 0$. The form factors of the separable perturbation are $\langle\mathbf{r}|\mathcal{F}_{s'}\rangle = \delta_{\text{reg}}(\mathbf{r} - \mathbf{R}_{s'})$, where $\delta_{\text{reg}}(\mathbf{r})$ is the Fermi-Huang

pseudopotential and the scatterer position $\mathbf{R}_{s'} = (0, 0, z_{s'})$ has the zero radial component (see Fig. 2). The Hamiltonian $\hat{H}$ is rotationally symmetric along the waveguide axis, and the perturbation affects only the states with zero angular momentum. Then, only products $|nl\rangle$ of the axially symmetric wave function $|n\rangle$ of two-dimensional harmonic oscillator and (for PBCs) a plane wave with the momentum $2\pi\hbar l/L$ are considered here. For a hard-wall box, the standing waves with the momentum $\pi\hbar l/L$ replace the plane waves (see [51]).

Unlike a flat billiard with a constant energy density of states, in the present model $E_\alpha \propto \alpha^{2/3}$, as for a three-dimensional free particle, and the energy density of states $\partial\alpha/E_\alpha \propto E_\alpha^{1/2}$ increases with the energy. The logarithmic asymptotic freedom [23] found for flat billiards is related to decreasing effective coupling $V_{\text{eff}} \propto 1/\log E$. However, it is a specific property of the systems with $E_\alpha \propto \alpha$. If $E_\alpha \propto \alpha^\gamma$ ($\gamma \neq 1$), one can see from the derivation [23] that $V_{\text{eff}} \propto E^{1-1/\gamma}$ has the same energy dependence as the energy difference between the states $\partial E_\alpha/\partial\alpha \propto E^{1-1/\gamma}$. Then, the present model, as well as a generic system with $\gamma \neq 1$, does not show the asymptotic freedom.

In the absence of the vector potential, $A = 0$, the energy spectrum of the integrable Hamiltonian is degenerate: $E_{nl} = E_{n-l}$. The degeneracy will be lifted by any potential with undefined parity. The vector potential lifts it as well, with no complication of the wave functions. However, the Hamiltonian loses the T invariance.

Four models are considered here. The nonsymmetric model is T noninvariant, and the scatterer positions $z_1 = 0$, $z_{s'} = (s' - 1 + \delta_{s'})L/s$ ($s' > 1$) have no symmetry due to random shifts $-0.25 \leq \delta_{s'} < 0.25$ chosen once for each s. The symmetric model with $z_{s-s'+1} = z_s - z_{s'}$ and equal $V_{s'}$ is PT invariant, where P is the inversion over $z_s/2$ (this model is not P invariant, as $\hat{H}_0$ is not P invariant if $A \neq 0$). The T-invariant model has $A = 0$ and the same scatterer positions as the nonsymmetric one. Only this model has degenerate E_{nl}. The three previous models correspond to PBCs, while the fourth, box model corresponds to the hard-wall box, has $A = 0$, and $z_{s'} = (s' + \delta_{s'})L/(s + 1)$.

Summation over l in Eq. (8) can be done analytically (see [51]), leaving a sum over $\sim E_\alpha/(\hbar\omega_\perp)$ values of n (the closed-channel contributions with $n\hbar\omega_\perp > E_\alpha$ decay exponentially with n). As $E_\alpha \propto \alpha^{2/3}$, calculation of the system (8) matrix and its solution requires $\sim s^2\alpha^{2/3}$ and $\sim s^3$ operations, respectively. Then α eigenstates are calculated for $\alpha \gg s^{3/2}$ with $\sim s\alpha^{5/3}$ operations (cf. with $\sim\alpha^3$ operations required by the direct diagonalization method).

The integrable system is described by two dimensionless parameters: $\lambda = mL^2\omega_\perp/\hbar$, characterizing the aspect ratio, and the scaled vector potential $l_0 = LA/(2\pi)$. In the calculations, $\lambda = \pi^3(1 + \sqrt{5}) \approx 100$ and $l_0 = 0.25 - e^{-4} \approx 0.232$ are expressed in terms of transcendent
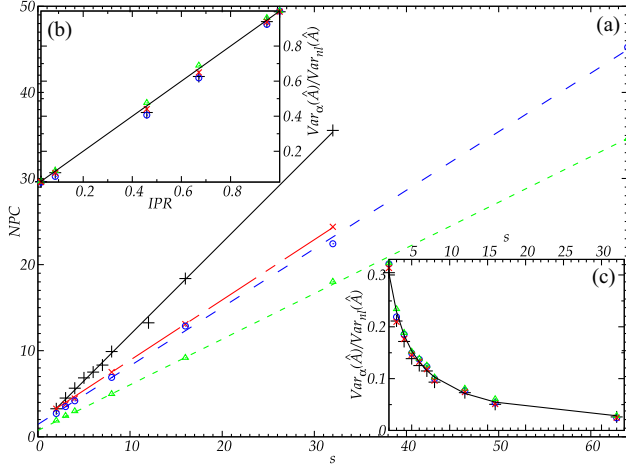
FIG. 3. (a) The dependence of the number of principal components on the number of scatterers for the nonsymmetric (pluses), symmetric (crosses), box (circles), and T-invariant (triangles) models in the unitary regime of strong perturbations. The lines represent the linear fits. (b) The ratio of variances over eigenstates of the nonsymmetric model with 32 scatterers to ones of the integrable system as a function of the inverse participation ratio on the change of the perturbation strength from the unitary regime to zero. (c) The same ratio as a function of the number of scatterers in the unitary regime. In (b) and (c), the symbols represent four observables, namely, the axial momentum (crosses), the part of the transverse potential energy in the total energy (pluses), and the occupations of the positive momenta (triangles) and of the odd axial modes (circles). The lines show IPR.

numbers. Approximately the same results are obtained for any $l_0 > 0.01$. In Figs. 3(a) and 3(c), $V_{s'} = 10^6 V_0$ for all scatterers is in the unitary regime ($V_0 = 2\pi\hbar^{5/2} m^{-3/2}\omega_\perp^{-1/2}$ is the scale of the interaction strength). Approximately the same results are obtained for any $V_{s'} > V_0$. In Fig. 3(b), $V_{s'}/V_0 = 10^6, 10^{-1}, 10^{-2}, 2 \times 10^{-3}, 10^{-3}, 10^{-4}, 0$ for the seven IPR values from left to right (the points for $V_{s'}/V_0 = 10^6$ and 10^{-1} are almost indistinguishable). Each point in Fig. 3 represents an average over the states $101 \leq \alpha \leq 10^6$ of the nonintegrable system.

The plots of NPC [see Fig. 3(a)] as a function of the number of scatterers for the four models confirm the linear dependence (6). The linear fits have two model-dependent parameters: η_2, which cannot be predicted by Eq. (6), since the system with a single scatterer is not chaotic enough, and ν. In Fig. 3(a), $\nu = 1.07$, 0.7, 0.68, and 0.53 for the nonsymmetric, symmetric, box, and T-invariant models, respectively. Taking into account the symmetry-dependent factors in Eq. (5), we can see that Γ' is approximately the same for the first three models.

The Lorentzian width is related to IPR by Eq. (5). Figure 3(a) demonstrates the linear dependence even when $\Gamma_s \sim \Delta E$. Therefore, even when the Fermi golden rule is inapplicable to Γ_s as the profile contains only a few energy

levels, the strength function can be approximated by the Lorentzian profile.

The physical implication of the rule (6) is related to the fluctuations of expectation values $\langle\alpha|\hat{O}|\alpha\rangle$ of an observable $\hat{O}$, characterized by their variance $\mathrm{Var}_\alpha(\hat{O}) = \overline{\langle\alpha|\hat{O}|\alpha\rangle^2} - \overline{\langle\alpha|\hat{O}|\alpha\rangle}^2$ over the eigenstates $|\alpha\rangle$. It is proportional to IPR and the variance for the underlying integrable system

$$\mathrm{Var}_\alpha(\hat{O}) = \eta\,\mathrm{Var}_\mathbf{n}(\hat{O}) \tag{10}$$

as was derived, in slightly different form, in Ref. [32]. The applicability criteria of this relation can be determined using the fact that it can also be derived in the same way as the relation between the initial, thermal, and relaxed expectation values (7) in Ref. [28] by replacing the density matrix by the observable. Then Eq. (10), like the relation (7) in Ref. [28], is applicable to perturbations with no selection rules. The relation (10) was compared with numerical results [32] for a many-body system with two-body interactions. However, such systems do have selection rules, as each two-body interaction conserves quantum numbers of other particles. It is probably the reason why the numerical results [32] were described by Eq. (10) only up to some energy-dependent factor. Systems with separable perturbations have no selection rules, and the relation (10) describes the dependence of variances on the number of scatterers and interaction strength for four observables [see Figs. 3(b) and 3(c)]. The observables are the axial momentum $\langle nl|\hat{p}_{\mathrm{ax}}|n'l'\rangle = l\delta_{n'n}\delta_{l'l}$, the occupation of positive momenta $\langle nl|\hat{P}_{\mathrm{pos}}|n'l'\rangle = \delta_{n'n}\delta_{l'l}\theta(l)$, the occupation of the odd axial modes $\langle nl|\hat{P}_{\mathrm{odd}}|n'l'\rangle = \delta_{n'n}\delta_{l'l}\delta_{l\,\mathrm{mod}\,2,1}$, and the part of the transverse potential energy $m\omega_\perp^2\rho^2/2$ in the total energy, $\langle nl|\hat{U}|n'l'\rangle = [(2n+1)\delta_{n'n} - (n+1)\delta_{n'n+1} - n\delta_{n'n-1}]\delta_{l'l}\hbar\omega_\perp/(2E_{nl})$. The averages and variances of these observable expectation values over the integrable system eigenstates are directly calculated. The averages are $\overline{\langle nl|\hat{p}_{\mathrm{ax}}|nl\rangle} = l_0$, $\overline{\langle nl|\hat{P}_{\mathrm{pos}}|nl\rangle} = 1/2$, $\overline{\langle nl|\hat{P}_{\mathrm{odd}}|nl\rangle} = 1/2$, and $\overline{\langle nl|\hat{U}|nl\rangle} = 1/3$. Although the average expectation value of the axial momentum is constant, its variation amplitude increases with the state energy. Then, the variance $\mathrm{Var}_{nl}(p_{\mathrm{ax}}) = mL^2(E_{\max}^{5/2} - E_{\min}^{5/2})/[10\pi^2\hbar^2(E_{\max}^{3/2} - E_{\min}^{3/2})]$ depends on the averaging interval $[E_{\min}, E_{\max}]$ boundaries. The variances for other observables are independent of the interval: $\mathrm{Var}_{nl}(\hat{P}_{\mathrm{pos}}) = 1/4$, $\mathrm{Var}_{nl}(\hat{P}_{\mathrm{odd}}) = 1/4$, and $\mathrm{Var}_{nl}(\hat{U}) = 1/45$. The expectation values over the nonintegrable system eigenstates are calculated using the expansion coefficients (7).

Together with Eq. (6), the relation (10) provides the decay of fluctuation variance on the increase of the number of scatterers, $\mathrm{Var}_\alpha(\hat{O}) = \mathrm{Var}_\mathbf{n}(\hat{O})/[\eta_2^{-1} + (s-2)\nu]$, or eigenstate thermalization approaching in a single-body system. Then, a set of fixed scatterers mimics the behavior

of many-body systems—sets of moving scatterers [65]. However, in many-body systems, the fluctuations decay exponentially with the number of particles. Then their chaoticity is extremely sensitive to the number of particles and the interaction strength. For fixed scatterers, the fluctuation decay is only inversely proportional to their number. This opens possibilities of fine control of the system chaoticity and exploration of the integrability-chaos crossover.

Chaotic properties of many-body systems of interacting particles are studied in numerous experimental and theoretical research. However, due to computational difficulties, a direct numerical simulation is performed for lattice systems (e.g., Refs. [14,17,19,31–33,37,38,40,41,44,47,48]) with a finite Hilbert space, while the problem complexity increases as a high power of the lattice site number and exponentially with the number of particles. A single particle in an external potential allows us to explore an infinite Hilbert space. Eigenstate thermalization has been analyzed [66] for 3×10^4 states of a Sinai-type billiard. However, the chaoticity of that system cannot be tuned, and the calculation of highly excited states is obstructed by the increase of the coordinate grid size. The properties of systems with several independent perturbations (particularly, scatterers) can be tuned by the number of perturbations and their strengths. Although the general results are confirmed by numerical calculations for a specific model, they are applicable to any integrable system, perturbed by several scatterers.

The predictions should be testable experimentally in several physical systems. Tightly trapped cold atoms of one kind can play the role of scatterers for an atom of a second kind in a wide trap. Moreover, several atoms of the second kind—with interactions between them turned off by a broad Feshbach resonance—can be used to get averages. In optics, photons in a cavity can be scattered by optical defects [67].

[1] G. Zaslavsky, *Chaos in Dynamic Systems* (Harwood, New York, 1985).

[2] T. Kinoshita, T. Wenger, and D. S. Weiss, A quantum Newton's cradle, Nature (London) **440**, 900 (2006).

[3] Y. Tang, W. Kao, K.-Y. Li, S. Seo, K. Mallayya, M. Rigol, S. Gopalakrishnan, and B. L. Lev, Thermalization near Integrability in a Dipolar Quantum Newton's Cradle, Phys. Rev. X **8**, 021030 (2018).

[4] A. Di Carli, C. D. Colquhoun, G. Henderson, S. Flannigan, G.-L. Oppo, A. J. Daley, S. Kuhr, and E. Haller, Excitation Modes of Bright Matter-Wave Solitons, Phys. Rev. Lett. **123**, 123602 (2019).

[5] D. Luo, Y. Jin, J. H. V. Nguyen, B. A. Malomed, O. V. Marchukov, V. A. Yurovsky, V. Dunjko, M. Olshanii, and R. G. Hulet, Creation and Characterization of Matter-Wave Breathers, Phys. Rev. Lett. **125**, 183902 (2020).

[6] I. Mazets, Integrability breakdown in longitudinaly trapped, one-dimensional bosonic gases, Eur. Phys. J. D **65**, 43 (2011).

[7] G. P. Brandino, J.-S. Caux, and R. M. Konik, Glimmers of a Quantum KAM Theorem: Insights from Quantum Quenches in One-Dimensional Bose Gases, Phys. Rev. X **5**, 041043 (2015).

[8] V. A. Yurovsky, B. A. Malomed, R. G. Hulet, and M. Olshanii, Dissociation of One-Dimensional Matter-Wave Breathers due to Quantum Many-Body Effects, Phys. Rev. Lett. **119**, 220401 (2017).

[9] O. V. Marchukov, B. A. Malomed, V. Dunjko, J. Ruhl, M. Olshanii, R. G. Hulet, and V. A. Yurovsky, Quantum Fluctuations of the Center of Mass and Relative Parameters of Nonlinear Schrödinger Breathers, Phys. Rev. Lett. **125**, 050405 (2020).

[10] N. L. Harshman, M. Olshanii, A. S. Dehkharghani, A. G. Volosniev, S. G. Jackson, and N. T. Zinner, Integrable Families of Hard-Core Particles with Unequal Masses in a One-Dimensional Harmonic Trap, Phys. Rev. X **7**, 041001 (2017).

[11] J. M. Deutsch, Quantum statistical mechanics in a closed system, Phys. Rev. A **43**, 2046 (1991).

[12] M. Srednicki, Chaos and quantum thermalization, Phys. Rev. E **50**, 888 (1994).

[13] M. Rigol, V. Dunjko, and M. Olshanii, Thermalization and its mechanism for generic isolated quantum systems, Nature (London) **452**, 854 (2008).

[14] A. Khodja, R. Steinigeweg, and J. Gemmer, Relevance of the eigenstate thermalization hypothesis for thermal relaxation, Phys. Rev. E **91**, 012120 (2015).

[15] A. M. Kaufman, M. E. Tai, A. Lukin, M. Rispoli, R. Schittko, P. M. Preiss, and M. Greiner, Quantum thermalization through entanglement in an isolated many-body system, Science **353**, 794 (2016).

[16] J. M. Deutsch, Eigenstate thermalization hypothesis, Reps. Prog. Phys. **81**, 082001 (2018).

[17] M. Rigol, V. Dunjko, V. Yurovsky, and M. Olshanii, Relaxation in a Completely Integrable Many-Body Quantum System: An Ab Initio Study of the Dynamics of the Highly Excited States of 1D Lattice Hard-Core Bosons, Phys. Rev. Lett. **98**, 050405 (2007).

[18] E. V. H. Doggen and J. J. Kinnunen, Quench-induced delocalization, New J. Phys. **16**, 113051 (2014).

[19] S. Nandy, A. Sen, A. Das, and A. Dhar, Eigenstate Gibbs ensemble in integrable quantum systems, Phys. Rev. B **94**, 245131 (2016).

[20] W. Verstraelen, D. Sels, and M. Wouters, Unitary work extraction from a generalized Gibbs ensemble using Bragg scattering, Phys. Rev. A **96**, 023605 (2017).

[21] C.-H. Wu, Time evolution and thermodynamics for a nonequilibrium system in phase-space, Can. J. Phys. **97**, 609 (2019).

[22] P. Šeba, Wave Chaos in Singular Quantum Billiard, Phys. Rev. Lett. **64**, 1855 (1990).

[23] T. Cheon and T. Shigehara, Scale anomaly and quantum chaos in billiards with pointlike scatterers, Phys. Rev. E **54**, 3300 (1996).

[24] O. Legrand, F. Mortessagne, and R. L. Weaver, Semiclassical analysis of spectral correlations in regular billiards with point scatterers, Phys. Rev. E **55**, 7741 (1997).

[25] W. G. Brown, L. F. Santos, D. J. Starling, and L. Viola, Quantum chaos, delocalization, and entanglement in

disordered Heisenberg models, Phys. Rev. E **77**, 021106 (2008).

[26] V. A. Yurovsky and M. Olshanii, Restricted thermalization for two interacting atoms in a multimode harmonic waveguide, Phys. Rev. A **81**, 043641 (2010).

[27] C. Stone, Y. A. E. Aoud, V. A. Yurovsky, and M. Olshanii, Two simple systems with cold atoms: Quantum chaos tests and non-equilibrium dynamics, New J. Phys. **12**, 055022 (2010).

[28] V. A. Yurovsky and M. Olshanii, Memory of the Initial Conditions in an Incompletely Chaotic Quantum System: Universal Predictions with Application to Cold Atoms, Phys. Rev. Lett. **106**, 025303 (2011).

[29] M. Kollar, F. A. Wolf, and M. Eckstein, Generalized Gibbs ensemble prediction of prethermalization plateaus and their relation to nonthermal steady states in integrable systems, Phys. Rev. B **84**, 054304 (2011).

[30] V. A. Yurovsky, A. Ben-Reuven, and M. Olshanii, Dynamics of relaxation and fluctuations of the equilibrium state in an incompletely chaotic system, J. Phys. Chem. B **115**, 5340 (2011).

[31] M. Olshanii, K. Jacobs, M. Rigol, V. Dunjko, H. Kennard, and V. A. Yurovsky, An exactly solvable model for the integrability-chaos transition in rough quantum billiards, Nat. Commun. **3**, 641 (2012).

[32] C. Neuenhahn and F. Marquardt, Thermalization of interacting fermions and delocalization in Fock space, Phys. Rev. E **85**, 060101(R) (2012).

[33] E. Canovi, D. Rossini, R. Fazio, G. E. Santoro, and A. Silva, Many-body localization and thermalization in the full probability distribution function of observables, New J. Phys. **14**, 095020 (2012).

[34] J. Larson, B. M. Anderson, and A. Altland, Chaos-driven dynamics in spin-orbit-coupled atomic gases, Phys. Rev. A **87**, 013624 (2013).

[35] L. Campos Venuti, S. Yeshwanth, and S. Haas, Equilibration times in clean and noisy systems, Phys. Rev. A **87**, 032108 (2013).

[36] O. Fialko, Decoherence via coupling to a finite quantum heat bath, J. Phys. B **47**, 045302 (2014).

[37] F. Andraschko, T. Enss, and J. Sirker, Purification and Many-Body Localization in Cold Atomic Gases, Phys. Rev. Lett. **113**, 217201 (2014).

[38] C. Khripkov, A. Vardi, and D. Cohen, Quantum thermalization: Anomalous slow relaxation due to percolation-like dynamics, New J. Phys. **17**, 023071 (2015).

[39] L. C. Venuti and P. Zanardi, Theory of temporal fluctuations in isolated quantum systems, Int. J. Mod. Phys. B **29**, 1530008 (2015).

[40] C. Khripkov, D. Cohen, and A. Vardi, Thermalization of bipartite Bose-Hubbard models, J. Phys. Chem. A **120**, 3136 (2016).

[41] C. Bartsch and J. Gemmer, Necessity of eigenstate thermalisation for equilibration towards unique expectation values when starting from generic initial states, Europhys. Lett. **118**, 10006 (2017).

[42] C. B. Dağ, S.-T. Wang, and L.-M. Duan, Classification of quench-dynamical behaviors in spinor condensates, Phys. Rev. A **97**, 023603 (2018).

[43] N. Yesha, Uniform distribution of eigenstates on a torus with two point scatterers, J. Spectr. Theory **8**, 1509 (2018).

[44] F. Iglói, B. Blaß, G. m. H. Roósz, and H. Rieger, Quantum XX model with competing short- and long-range interactions: Phases and phase transitions in and out of equilibrium, Phys. Rev. B **98**, 184415 (2018).

[45] T. Goldfriend and J. Kurchan, Equilibration of quasi-integrable systems, Phys. Rev. E **99**, 022146 (2019).

[46] A. Bastianello, Lack of thermalization for integrability-breaking impurities, Europhys. Lett. **125**, 20001 (2019).

[47] W.-J. Huang, Y.-B. Wu, G.-C. Guo, and X.-B. Zou, Ergodic-nonergodic transition with cold spinless fermions in a cavity, Phys. Rev. A **105**, 033315 (2022).

[48] J.-L. Ma, Q. Li, and L. Tan, Ergodic and nonergodic phases in a one-dimensional clean Jaynes-Cummings-Hubbard system with detuning, Phys. Rev. B **105**, 165432 (2022).

[49] P. Sierant and J. Zakrzewski, Challenges to observation of many-body localization, Phys. Rev. B **105**, 224203 (2022).

[50] B. Georgeot and D. L. Shepelyansky, Breit-Wigner Width and Inverse Participation Ratio in Finite Interacting Fermi Systems, Phys. Rev. Lett. **79**, 4365 (1997).

[51] See Supplemental Material at http://link.aps.org/supplemental/10.1103/PhysRevLett.130.020404, which includes Refs. [52–55], for derivation details.

[52] DLMF, NIST Digital Library of Mathematical Functions, http://dlmf.nist.gov/, release 1.1.6 of 2022-06-30, edited by F. W. J. Olver, A. B. Olde Daalhuis, D. W. Lozier, B. I. Schneider, R. F. Boisvert, C. W. Clark, B. R. Miller, B. V. Saunders, H. S. Cohl, and M. A. McClain.

[53] J. Avery, *Hyperspherical Harmonics: Applications in Quantum Theory* (World Scientific, London, 2017).

[54] A. Prudnikov, Y. Brychkov, and O. Marichev, *Integrals and Series, Vol. I: Elementary Functions* (Taylor and Francis, London, 1998).

[55] M. G. Moore, T. Bergeman, and M. Olshanii, Scattering in tight atom waveguides, J. Phys. IV (France) **116**, 69 (2004).

[56] M. V. Berry, Regular and irregular semiclassical wavefunctions, J. Phys. A **10**, 2083 (1977).

[57] S. A. van Langen, P. W. Brouwer, and C. W. J. Beenakker, Fluctuating phase rigidity for a quantum chaotic system with partially broken time-reversal symmetry, Phys. Rev. E **55**, R1 (1997).

[58] E. P. Wigner, Characteristic vectors of bordered matrices with infinite dimensions, Ann. Math. **62**, 548 (1955).

[59] Y. V. Fyodorov and A. D. Mirlin, Statistical properties of random banded matrices with strongly fluctuating diagonal elements, Phys. Rev. B **52**, R11580 (1995).

[60] K. Frahm and A. Müller-Groeling, Analytical results for random band matrices with preferential basis, Europhys. Lett. **32**, 385 (1995).

[61] P. Jacquod and D. L. Shepelyansky, Hidden Breit-Wigner Distribution and Other Properties of Random Matrices with Preferential Basis, Phys. Rev. Lett. **75**, 3501 (1995).

[62] Q. Guan, V. Klinkhamer, R. Klemt, J. H. Becher, A. Bergschneider, P. M. Preiss, S. Jochim, and D. Blume, Density Oscillations Induced by Individual Ultracold Two-Body Collisions, Phys. Rev. Lett. **122**, 083401 (2019).

[63] A. Derevianko, Anisotropic pseudopotential for polarized dilute quantum gases, Phys. Rev. A **67**, 033607 (2003); Erratum, Phys. Rev. A **72**, 039901 (2005).

[64] K. Kanjilal, J. L. Bohn, and D. Blume, Pseudopotential treatment of two aligned dipoles under external harmonic confinement, Phys. Rev. A **75**, 052705 (2007).

[65] A similar analogy between classical counterparts—2D problem of fixed scatterers and the hard sphere gas—was considered in Ref. [1]. But, to my best knowledge, no quantitative relationship between the number of scatterers and characteristics of classic chaos is known.

[66] A. H. Barnett, Asymptotic rate of quantum ergodicity in chaotic Euclidean billiards, Commun. Pure Appl. Math. **59**, 1457 (2006).

[67] R. Bruck, C. Liu, O. L. Muskens, A. Fratalocchi, and A. Di Falco, Ultrafast all-optical order-to-chaos transition in silicon photonic crystal chips, Laser Photonics Rev. **10**, 688 (2016).